Journal of The Electrochemical Society, **162** (3) F243-F249 (2015)
0013-4651/2015/162(3)/F243/7/$31.00 © The Electrochemical Society

Promoting Effect of Tin in Platinum Electrocatalysts for Direct Methanol Fuel Cells (DMFC)

Natalia S. Veizaga,[a,z] Virginia I. Rodriguez,[a] Thairo A. Rocha,[b] Mariano Bruno,[c] Osvaldo A. Scelza,[a] Sergio R. de Miguel,[a] and Ernesto R. Gonzalez[b,*]

[a]*Instituto de Investigaciones en Catálisis y Petroquímica "Ing. José Miguel Parera" (INCAPE), Universidad Nacional del Litoral-CONICET, 3000 Santa Fe, Argentina*
[b]*Instituto de Química de São Carlos, CP 780 São Carlos, SP, Brazil*
[c]*Departamento de Física de la Materia Condensada, Centro Atómico Constituyente, Comisión Nacional de Energía Atómica (CNEA), 1650 Buenos Aires, Argentina*

Pt-Sn anodic catalysts supported on multiwall carbon nanotubes, mesoporous carbon and Vulcan carbon were prepared using a deposition-reduction technique with sodium borohydride, characterized by different techniques and tested as anodes in a single direct methanol fuel cell at low temperatures. Characterization and CO stripping results indicate the presence of promoting effects of Sn over Pt in catalysts supported on Vulcan carbon and carbon nanotubes. This would mainly be caused both by geometric modifications induced by Sn placed in the surroundings of the active metal phase and probable electronic effects. These promoting effects make the oxidation of CO to CO_2 at low potentials easier, thus improving the CO tolerance of the anodic electrocatalyst. On the other hand, Pt-Sn catalysts supported on mesoporous carbon do not show a proper metallic phase needed for a good electrochemical behavior. When catalysts were tested in a DMFC, Pt-Sn catalysts supported on Vulcan carbon and carbon nanotubes gave a better power density than a commercial one mainly when working at low current densities.

Manuscript submitted August 14, 2014; revised manuscript received December 2, 2014. Published December 12, 2014.

Low temperature Direct Alcohol Fuel Cells (DAFCs) are extremely attractive as power sources for transportation, mobile and portable applications.[1] Compared to hydrogen-fed fuel cells, which need to employ reforming technology and/or require hydrogen storage, DAFCs use a simple liquid fuel. Methanol is a promising fuel because it is an easily oxidized alcohol, and thus direct methanol fuel cells (DMFCs) have been developed for the portable power market.[2,3]

Methanol oxidation has been reported to involve the adsorption of CH_3OH followed by successive dehydrogenation steps, yielding linearly bonded CO. At sufficiently anodic potentials, the adsorbed carbon monoxide, CO_{ads}, is believed to react with an adsorbed OH_{ads} intermediate. In general, it has been shown that pure Pt systems are not efficient catalysts for the oxidation of methanol because Pt is rapidly poisoned by the CO species produced as oxidation intermediates. For this reason, the modification of Pt electrode with other metals including Ru, Sn, Mo and Sb has been investigated extensively.[4–22] In order to achieve maximum tolerance of the platinum catalyst to CO poisoning, it is important that the second metal is in contact with platinum. In these catalysts, the second metal will provide O-species for CO removal from the Pt active sites.

Among many bimetallic Pt based catalysts that have been considered for CO tolerance, Pt-Ru ones certainly are the most studied, with PtRu(1:1) catalyst showing a high CO tolerance. The use of Pt-Ru/C as an oxidation catalyst for H_2 containing CO at the anode, leads to a lowering of the CO oxidation potential compared with that of Pt/C catalyst.

On the other hand, for Pt-Sn(3:1)/C, it has been reported that the onset potential of CO oxidation was shifted toward more negative side compared to that of the Pt-Ru (1:1).[23] It can thus be expected that there seems to be a possibility of using the Pt-Sn/C as a CO filter.

Pt–Sn/carbon nanocomposites, prepared by different electrochemical or chemical deposition methods have been studied as anode catalysts for the electro-oxidation of methanol and other small molecule fuels.[24–31] It is well known that catalytic activity of a metal strongly depends on its particle shape and size distribution.[32]

One strategy to effectively disperse catalytic particles is to explore novel carbon materials. Several research groups have demonstrated that carbon nanotubes can more effectively improve the electrocatalytic activity of Pt catalysts compared to the most widely used carbon support, Vulcan carbon.[33] Recently, mesoporous carbon with tailored structure has been used as a support for fuel cell catalyst, exhibiting promising activities both in half cell or single cell configuration.[34–39]

In this paper, Pt-Sn catalysts supported on multiwall carbon nanotubes, mesoporous carbon and Vulcan carbon were prepared using chemical reduction with sodium borohydride, studied by cyclic voltammetry and tested as anodes in single direct methanol fuel cells at low temperatures in order to identify the most appropriate support for this electrocatalyst. The objective of the paper is to compare Pt-Sn bimetallic catalysts supported on different carbons (nanotubes, mesoporous and Vulcan) with a commercial one in a working DMFC.

The supported metallic phases were characterized by temperature programmed reduction, X-ray photoelectron spectroscopy, H_2 chemisorption, benzene hydrogenation reaction, transmission electron microscopy, CO stripping and chronoamperometry.

Experimental

Electrocatalyst preparation.— The carbonaceous supports used for the catalyst preparation were Vulcan carbon (VC), multiwall carbon nanotubes (NT) and mesoporous carbon (MC). Vulcan carbon XC-72 has a specific surface area (S_{BET}) of 240 $m^2\ g^{-1}$, a pore volume (V_{pore}) of 0.31 $cm^3\ g^{-1}$ and a mean particle size of 40 nm. Commercial multiwall carbon nanotubes (MWCN from Sunnano, purity >90%, diameter: 10–30 nm, length: 1–10 μm) with the following textural properties: $S_{BET} = 211\ m^2\ g^{-1}$ and $V_{pore} = 0.46\ cm^3\ g^{-1}$, were used. The physical properties of the structured mesoporous carbon were: $S_{BET} = 476\ m^2\ g^{-1}$ and $V_{pore} = 0.35\ cm^3\ g^{-1}$. A maximum in the pore size distribution is found at around 9 nm for MC. The micro- (<2 nm) and meso-porosity (between 2 and 50 nm) is attributed to the structure of the carbon, which consists of clusters of porous uniform spheres in a fairly regular array. Therefore, the obtained material has a hierarchical pore structure (micro- and mesoporosity).[40,41] The metallic precursors were $H_2PtCl_6.6H_2O$ (Tetrahedron, analytical grade) and $SnCl_2.2H_2O$ (Cicarelli, analytical grade). Catalysts were prepared by deposition-reduction technique in liquid phase (called RB) using $NaBH_4$ (Merck, analytical grade) as reducing agent.

The supports were dispersed into water and stirred for 30 min at 40°C. Then, calculated amounts of H_2PtCl_6 and $SnCl_2.2H_2O$ solutions were added to the above mixture and stirred for 30 min. A freshly prepared 0.4 M $NaBH_4$ solution (in 1 M NaOH) was added drop by drop into the above solution under vigorous stirring in four portions of the same volume. The portions were added after 30 min one from the other. After stirring for 1 h, the obtained mixture was cooled up

*Electrochemical Society Active Member.
[z]E-mail: nveizaga@fiq.unl.edu.ar

to room temperature, filtered and washed repeatedly with deionized water. The formed powder was dried at 70°C for 3 h in a vacuum oven. All the prepared samples consisted of 17 wt% Pt and a molar ratio Sn/Pt = 0.33. For comparison, monometallic Pt catalysts were also prepared by the $NaBH_4$ reduction process.

Characterization of the supports and electrocatalysts.— Temperature programmed reduction (TPR).— After deposition of the metals, catalysts previously dried under vacuum at 60°C were reduced by using a reductive mixture (10 mL min^{-1} of H_2 (5 %v/v)-N_2) in a flow reactor. Samples were heated at 6°C min^{-1} from 25°C to 800°C. The exit of the reactor was connected to a TCD in order to obtain the TPR signal.

X Ray photoelectron spectroscopy (XPS).—XPS measurements were carried out in a Multitechnic Specs Photoemission Electron Spectrometer equipped with an X-ray source Mg/Al and a hemispherical analyzer PHOIBOS 150 in the fixed analyzer transmission (FAT) mode. The spectrometer operates with an energy power of 100 eV and the spectra were obtained with a pass energy of 30 eV and a Mg anode operated at 90 W. The analysis chamber was kept at pressure lower than 1.5×10^{-8} torr. The binding energies (BEs) of the signals were referred to the C1s peak at 284 eV. Peak areas values were estimated by fitting the signals with a combination of Lorentzian–Gaussian curves of variable proportion and using the CasaXPS Peak fit software version 1.

H_2 chemisorption.—The H_2 chemisorption measurements were made in a volumetric equipment at room temperature. The sample weight used on the experiments was 100 mg, this being previously outgassed under vacuum (10^{-4} Torr). The H_2 adsorption isotherms were obtained between 25 and 100 Torr. The isotherms were linear in the range of used pressures and the H_2 chemisorption capacities were calculated by extrapolation of the isotherms to zero pressure.[42]

Benzene hydrogenation reaction.—The test reaction of the metallic phase (benzene -Bz- hydrogenation) was carried out in a differential flow reactor at 110°C. In this case a molar ratio $H_2/Bz = 26$ and a volumetric rate of 600 mL min^{-1} were used. The sample weight was such as to obtain a conversion lower than 5% (10–20 mg). The activation energy in benzene hydrogenation for different catalysts was obtained by measuring the initial reaction rate at 110, 100 and 90°C. The reaction products were analyzed by using a gas chromatographic system (packed column with Chromosorb and FID as detector).

Transmission electron microscopy (TEM).—TEM measurements were carried out on a JEOL 100CX microscope, operated with an acceleration voltage of 100 kV, and magnification ranges of 80,000 × and 100,000 ×. For each catalyst, approximately 200 particles were observed and the distribution of particle sizes was done on this basis. The mean particle diameter (d) was calculated as: $d = \Sigma(ni.d_i)/\Sigma ni$; where ni is the number of particles of diameter di.

CO stripping.—Catalysts were characterized by means of CO stripping (electrochemical characterization) in a conventional cell with three electrodes, using a potentiostat/galvanostat (TEQ-02, Argentina). Pure CO is bubbled in an electrolytic solution of 0.5 M H_2SO_4. CO is quickly adsorbed on the Pt surface producing a CO adsorbed monolayer. During the CO adsorption process (1 h), the potential of the cell is maintained constant at 200 mV (this value is lower than the CO oxidation potential). Then, an inert gas (N_2) is passed to purge the electrolytic solution in order to eliminate the dissolved CO, thus only the adsorbed CO remains on the Pt surface. In these conditions, and maintaining constant the flow of inert gas, the potential was modified in order to induce the CO oxidation. When the Pt surface is covered by a monolayer of CO, the hydrogen adsorption is inhibited. Hence the typical H_2 adsorption and desorption peaks do not appear in the cyclic voltammograms. When the CO monolayer is removed by oxidation at high potentials, the Pt surface is able to adsorb and desorb H_2, thus appearing the corresponding peaks. In order to observe the process of occupation and releasing of the Pt active sites by CO, the potentials of the voltammetry are programmed so that the potential starts at open circuit under N_2 atmosphere and it is cycled between -200 and 1200 mV (vs. Ag/AgCl). In this way in the first cycle, the H_2 adsorption-desorption characteristic peaks are not detected and at higher potentials the CO stripping peak is produced by oxidation of CO to CO_2 which is released from the Pt surface. In the second cycle the characteristic peaks of H_2 are clearly observed and they correspond to those observed in a conventional voltammetry of a Pt electrode in contact with H_2.

The specific electrochemical active area (EASS) -Eq. 1- is an important parameter for the comparison of the electroactivity of the catalysts. This parameter is obtained from the CO voltammetry (CO desorption peak) as:

$$EASS = \frac{(Q_{CO}/q^s_{CO})}{m_{Pt}} \quad [1]$$

where m_{Pt} is the Pt mass, Q_{CO} is the charge required for the oxidation of the monolayer of CO adsorbed on the active sites, and q^s_{CO} is a reference value equal to 0.42 mC cm^{-2} (assuming that the surface density of polycrystalline Pt is 1.3 10^{15} atoms cm^2 and that each CO molecule is adsorbed on a single Pt atom, and two electrons are involved in the oxidation of CO to CO_2).[43]

Chronoamperometry measurements.—The tests were carried out to evaluate the effect of the electrode potential on methanol oxidation in solutions of 0.5 M H_2SO_4 and 1 M CH_3OH for 3600 s. The potential was fixed at 350 mV.

Tests in a DMFC cell.—All electrodes were made to contain 1 mg Pt cm^{-2}. A commercial Pt/VC E-TEK 30 wt% was used in the cathode, while the bimetallic Pt-Sn catalysts prepared by deposition-reduction in liquid phase were used in the anode. The experiments in the DMFC were carried out in two conditions: at 70°C and atmospheric pressure of O_2 in the cathode, and at 90°C and 2 atm of O_2 in the cathode. The geometric area of the electrodes was 4.62 cm^2. In all cases, a Nafion 115 membrane was used as electrolyte. The membrane and electrode assemblies (MEAs) were prepared by hot-pressing two electrodes on both sides of a pre-treated Nafion 115 membrane (H^+, DuPont) at 125°C and 5 MPa for 2 min. The MEA was placed between two high-density carbon plates in which serpentine-type channels were machined for the circulation of O_2 (70 mL min^{-1}) and a methanol solution (2M). The commercial catalyst used to compare the performance was Pt/VC E-TEK 20 wt%.

Results and Discussion

Figure 1 shows temperature programmed reduction profiles (TPR) of the different Pt-Sn catalysts prepared by deposition-reduction in liquid phase by sodium borohydride (RB) and supported on different carbonaceous materials (Vulcan carbon, carbon nanotubes and mesoporous carbon). For the sake of comparison, the TPR profile of a monometallic Pt catalyst prepared by conventional impregnation (CI) and supported on the corresponding carbon is added in each figure. It is important to notice that the TPR profiles of Pt-Sn catalysts supported on VC, NT and MC do not show practically any reduction peak in the zone where Pt is reduced in the impregnated catalysts (at about 230°C). This would indicate that the major fraction of Pt would be in metallic state (Pt^0). However, nothing can be said about the reducibility state of Sn. It is also observed that Pt-Sn/MC shows an important hydrogen consumption zone at high temperature due to the reduction of surface oxygen groups of the mesoporous carbon.[44]

In order to find more information about the Pt and Sn reducibilities of the bimetallic catalysts supported on VC and NT, a XPS characterization was done. From the deconvolution of Pt4f spectra (Figure 2) of the different samples, a peak at 71.8 eV was obtained for the Pt $4f_{7/2}$ signal and another peak at 75.0 eV for Pt $4f_{5/2}$. These peaks correspond to the zerovalent state of Pt. Two additional small doublets are also observed in Figure 2, one at 74.3 eV and 77.8 eV and the other one at 75.5 eV and 78.4 - 78.8 eV, that belong to the corresponding oxides or oxychlorides of Pt.[45] In each case, the concentration of the surface oxidized species was lower than 35%, this meaning that most of Pt surface species (>65%) are in metallic state

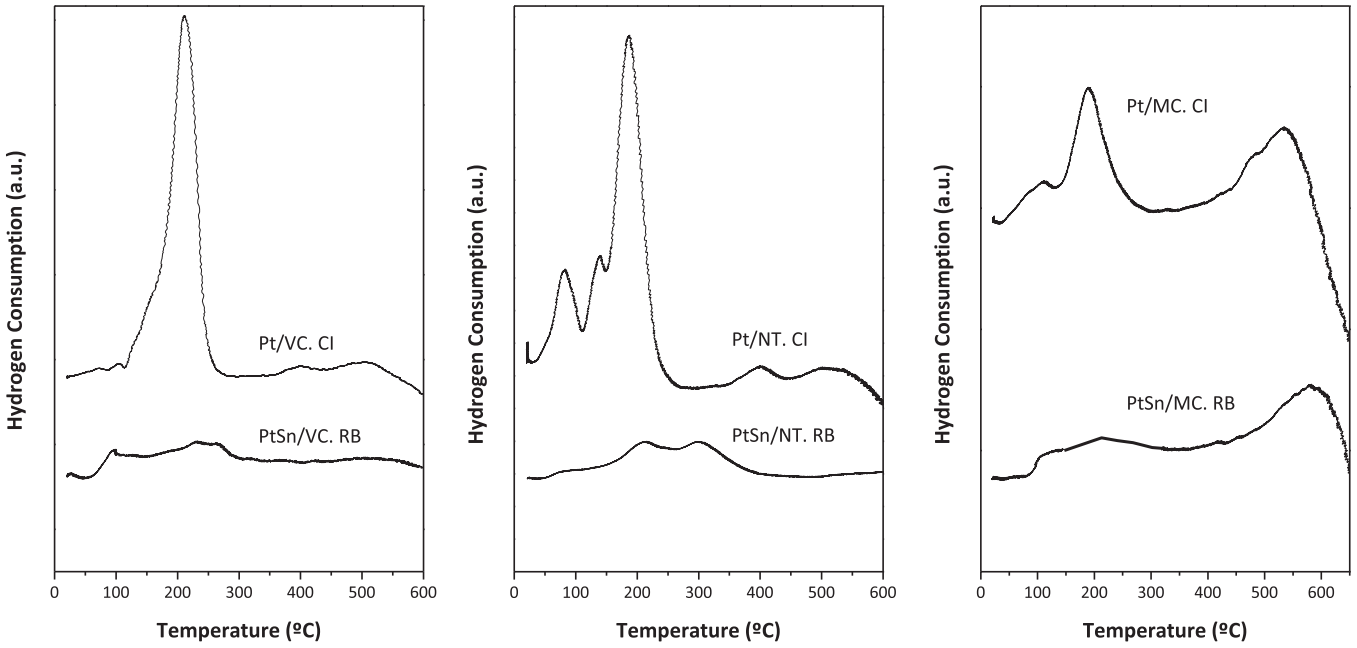

Figure 1. TPR profiles of Pt-Sn bimetallic catalysts supported on VC, NT and MC and prepared by RB and CI.

in the catalysts supported on VC and NT. XPS of Sn3d (Figure 2) shows that Sn forms oxidized species and only a small proportion of Sn^0 (10–15%) was found, this small metallic fraction perhaps forming alloys with metallic Pt. A similar behavior of the reducibility of the metals was also found for the Pt-Sn/MC catalyst.

Hydrogen chemisorption capacities of Pt and Pt-Sn catalyst series are shown in Table I. Even though the bimetallic catalyst supported on VC showed chemisorption values higher than the corresponding monometallic catalyst, the similar catalyst supported on NT showed similar values to the corresponding monometallic one. A different behavior was observed for the bimetallic catalyst supported on MC since its chemisorption value is noticeable lower than the corresponding monometallic one, this indicating an influence of the support type on the structure of the deposited metallic phase. It is worth noticing that, besides this supporting effect, other electronic and geometrical effects could be produced due to the influence of the promotor (Sn) in the vicinity of Pt as well. These additional effects are more noticeable for the series supported on the mesoporous carbon whose chemisorptive capacity is highly reduced, probably due to a blocking effect.

Benzene hydrogenation is a structure-insensitive reaction, which can be carried out on one active metallic site.[46,47] The changes in the

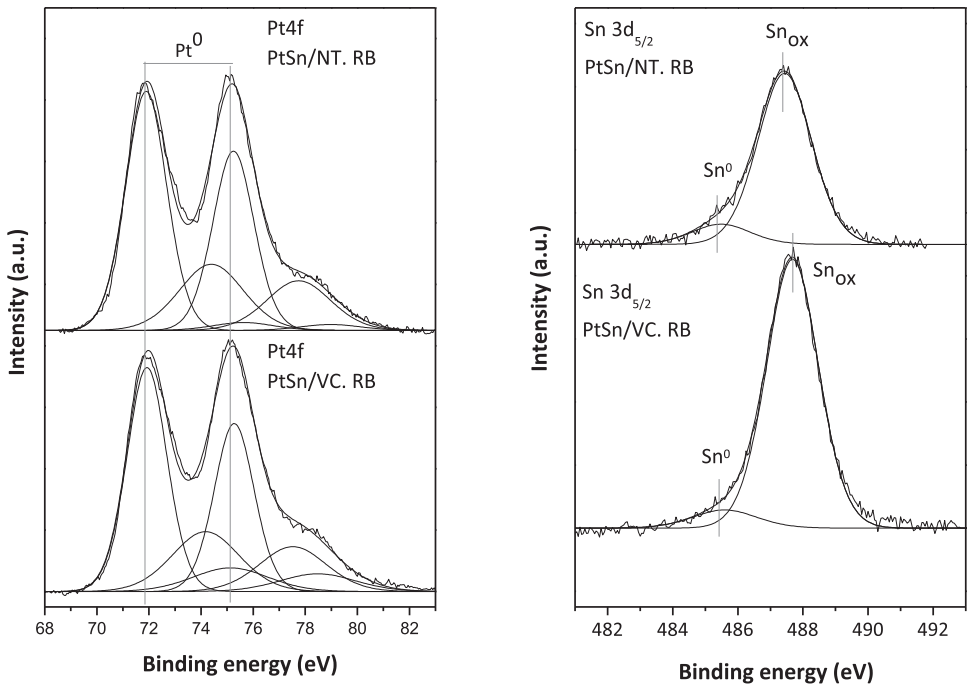

Figure 2. Pt 4f and Sn 3d XPS signals of Pt-Sn catalysts supported on VC and NT prepared by liquid phase reduction method with 0.4 M $NaBH_4$.

Table I. Hydrogen chemisorption and activation energy values (Ea_{Bz}) in benzene hydrogenation reaction at 110°C for bimetallic catalyst series and for the corresponding monometallic catalysts.

Catalyst	Hydrogen Chemisorption (μmol H_2/ g cat)	Benzene Hydrogenation Ea_{Bz} (Kcal/mol)
Pt/VC. RB	138	10
PtSn/VC. RB	196	15
Pt/NT. RB	83	14
PtSn/NT. RB	75	11
Pt/MC. RB	212	12
PtSn/MC. RB	95	13

Table II. Onset potential of CO oxidation and electrochemically active specific surface (EASS) for PtSn catalysts supported on different carbonaceous materials obtained by CO stripping voltammetry.

Catalyst	Onset potential of CO oxidation (mV)	EASS (m^2/g Pt)
Pt/VC. RB	407	12
PtSn/VC. RB	136	14
Pt/NT. RB	330	31
PtSn/NT. RB	140	15
Pt/MC. RB	429	48
PtSn/MC. RB	ud	ud

ud: undetected.

activation energies (Ea_{Bz}) can be related to electronic modifications of the active sites. This test reaction of the metallic phase can be used for the characterization of catalysts prepared by deposition-reduction in liquid phase at low temperature, since the temperature used for this reaction is also low (100–130°C), and in these conditions there would be no changes in the characteristics of the catalysts by the temperature. Table I also shows the results of activation energies in benzene hydrogenation for the different mono and bimetallic catalysts prepared by deposition-reduction with sodium borohydride. The activation energy value of the Pt-Sn catalyst is higher than the corresponding monometallic one only in the case of the series supported on Vulcan carbon. This would indicate that electronic effects are more important in the Pt-Sn/VC catalyst. Hence, the important decrease of the chemisorption capacity in the Pt-Sn/MC catalyst would be caused only by geometric effects, viz. the blocking of Pt by the second metal.

Figure 3 shows the cyclic voltammograms of CO stripping corresponding to mono and bimetallic catalysts supported on VC, NT and MC. The Pt/VC catalyst shows a main CO oxidation peak at about 0.51 V vs. Ag/AgCl, this value being similar to the one found by Vidakovic et al.[48] and reported as 0.536 V vs. Ag/AgCl for the CO stripping potential peak of a supported Pt catalyst. In the Pt-Sn electrocatalyst supported on VC, the CO oxidation peak is divided. A main peak appears at similar potential than in the monometallic catalyst, which can be due to the oxidation of strongly adsorbed CO on the metallic sites. Besides, a small peak at 0.20 V vs. Ag/AgCl is also observed, which can be attributed to the oxidation of CO species weakly adsorbed on other metallic sites probably modified by the presence of the second metal in the vicinity of Pt. For the bimetallic catalyst the onset potential is found at 0.1 V, whereas that of the monometallic one is placed at 0.4 V vs. Ag/AgCl. It is clearly evidenced an important promoting effect of Sn, which shifts the CO oxidation to lower potentials (Figure 3a). Similar effects as the ones observed for the VC supported catalysts are found for NT supported ones (Figure 3b). In this sense, for the monometallic Pt/NT catalyst the onset potential is at 0.33 V, and it is found to be at lower potentials (0.1 V) for Pt-Sn/NT catalyst. The monometallic catalyst displays a wide oxidation peak with a maximum between 0.51 and 0.54 V vs. Ag/AgCl, but the Pt-Sn/NT catalyst shows an oxidation peak similar to the monometallic one and another oxidation peak or shoulder at lower potentials (0.33 V vs. Ag/AgCl). In this series an important promoting effect of Sn over Pt is observed, thus improving the CO tolerance of the anodic electrocatalyst.

With respect to the Pt-Sn/MC catalyst, the cyclic voltammograms of CO oxidation (Figure 3c) show no CO oxidation peak, probably due to important blocking effects of Sn over the active metal, this agreeing with the important decrease of the hydrogen chemisorption capacity (see Table I). Summarizing, these bimetallic systems of Pt-Sn prepared by RB and supported on mesoporous carbon do not show a proper metallic phase needed to develop a good electrochemical behavior.

Table II shows the onset potencial of CO oxidation and electrochemical areas of bimetallic catalysts compared with those of the corresponding monometallic ones. It is clearly observed that the beginning of the CO oxidation is shifted to lower potentials for Pt-Sn

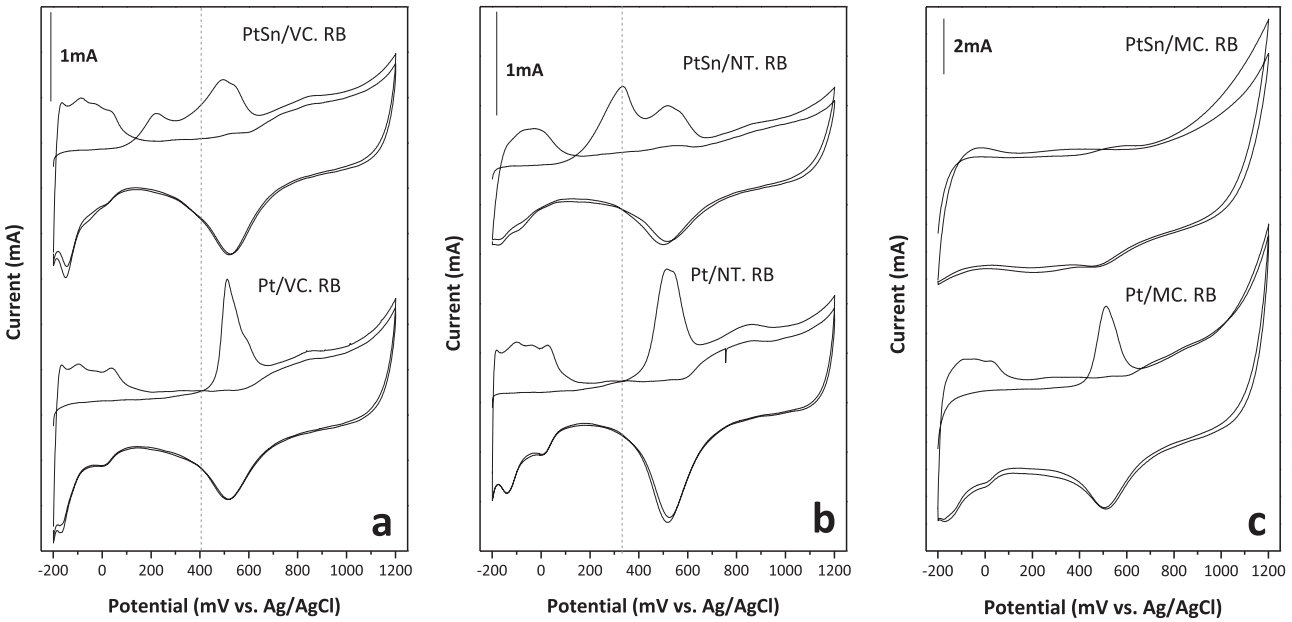

Figure 3. Cyclic CO stripping voltammograms for Pt and Pt-Sn catalysts supported on a) VC, b) NT, and c) MC. Electrolytic solution: 0.5 M H_2SO_4.

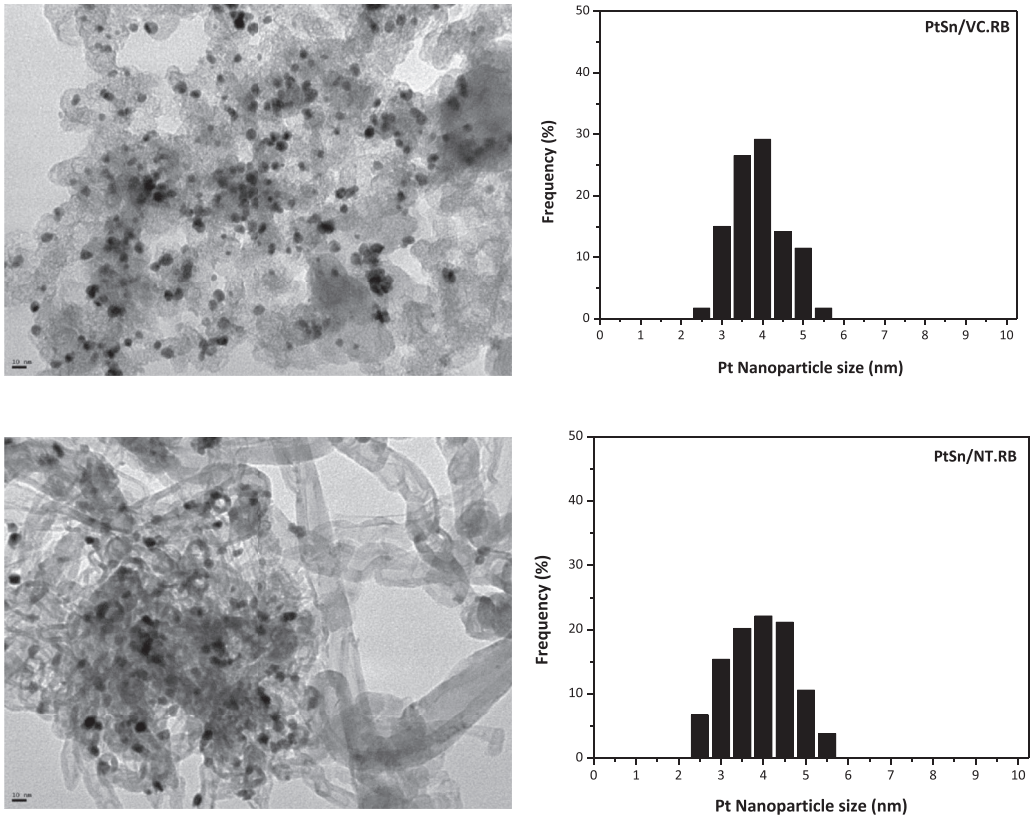

Figure 4. TEM images of bimetallic Pt-Sn catalysts supported on VC and NT and the corresponding size particle distribution histograms.

catalysts supported on VC and NT. Regarding the values of electrochemically active specific surface (EASS) shown in Table II (obtained from CO stripping tests), it can be observed that the Pt-Sn catalyst supported on VC does not modify these values with respect to Pt/VC one, while the EASS value for bimetallic catalyst supported on NT shows a decrease that would be caused by the geometric effects of Sn over active Pt sites.

The earlier oxidation of CO_{ads} in Sn containing electrodes, compared with the corresponding Pt one, could be explained by the Sn ability of adsorbing OH at more negative potentials than Pt and by the reactions of surrounding CO_{ads} species over Pt sites (bifunctional mechanism) or by the modification of the d electronic Pt bands by Sn as well.[25] In this sense, characterization and CO stripping results would be indicating that there exist promoting effects of Sn over Pt in catalysts supported on VC and NT. This could be explained by geometric modifications caused by the promoter placed in the vicinity of the active metallic phase, even though Sn electronic modifications over Pt (specially on Vulcan carbon) should not be discarded.

Finally, Pt-Sn catalysts prepared on VC and NT were characterized by TEM (Figure 4) and size particle distributions (2.5 to 5.5 nm) with similar mean particle sizes in VC and NT samples of 3.7 nm were found. These particle distributions were narrower than those obtained for the corresponding monometallic catalysts. In this sense, Pt/VC and Pt/NT catalysts show a wide range of Pt particle size distribution from 3 to 10 nm with an average particle size of 6 and 5 nm, respectively, as it was previously described by Veizaga et al.[44] This indicates that the presence of Sn modifies Pt during the deposition-reduction with sodium borohydride, reducing the particle size and leading to a narrower size distribution (shown by TEM) than the corresponding monometallic catalysts supported on VC and NT.

Characterization and CO stripping results are indicating promoting effects of Sn over Pt in catalysts supported on VC and NT. This would mainly be caused both by geometric modifications induced by Sn placed in the surroundings of the active metal phase and the existence of probable electronic effects. These promoting effects would ease the oxidation of CO to CO_2 at low potentials.

In order to test the behavior of Pt-Sn/VC and Pt-Sn/NT catalysts in methanol electro-oxidation, chronoamperometry measurements at 350 mV were carried out in solutions of 0.5 M H_2SO_4 and 1M CH_3OH for 3600 s. Figure 5 shows the curves of current intensity versus time. As it can be seen, there is an initial step in which the current quickly falls before 10 min, then the current gradually falls with time and finally it remains constant. These currents at high reaction times can characterize an equilibrium state of methanol adsorption and

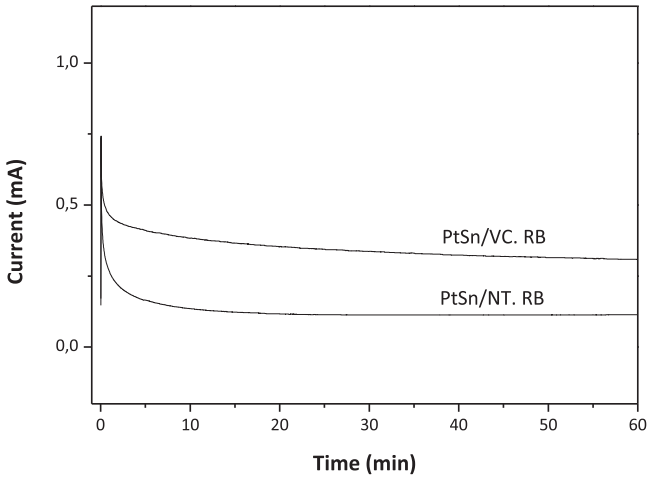

Figure 5. Current–time curves recorded in a 0.5 M H_2SO_4 + 1 M CH_3OH solution at E = 0.35 V.

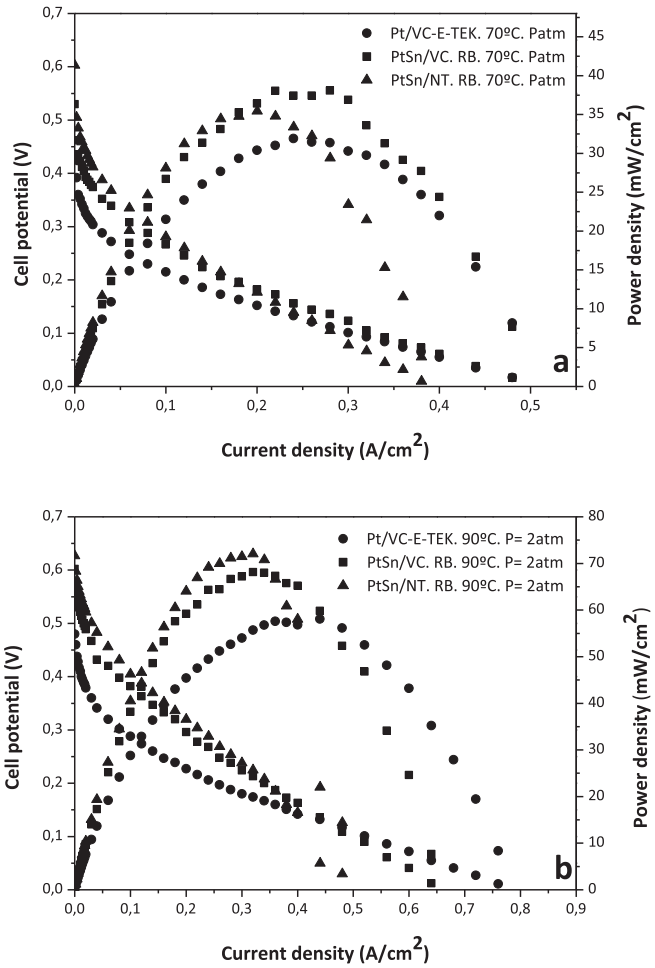

Figure 6. Polarization and current density curves in a DMFC for Pt-Sn/VC. RB and Pt-Sn/NT. RB anodic catalysts compared to commercial Pt/VC (E-TEK 20%wt) catalyst. As cathodic catalyst it was used a Pt/VC (E-TEK 30%wt) one. a) 70°C, 1atm O_2 pressure, b) 90°C, 2 atm O_2 pressure. 2 M methanol solution. The Pt loading was 1 mg cm^{-2} for both the anode and cathode.

electro-oxidation. It can be seen that Pt-Sn/VC catalyst reaches higher current intensity in stationary state than Pt-Sn/NT.

By using chronoamperometric experiments, Neto et al.[49] showed that the Pt-Sn/C electrocatalyst was more active than the Pt-Ru/C and Pt-Ru-Sn/C electrocatalysts for methanol and ethanol oxidation at room temperature. The superior performance of the Pt-Sn/C electrocatalyst for methanol and ethanol oxidation could be due to the fact that only part of the tin amount was found as a PtSn alloy, which changes the Pt electronic properties and probably "tunes" the ability of Pt to adsorb methanol or ethanol and dissociate C-H bonds, while the other part found as SnO_2 species facilitates the oxidation of adsorbed CO formed as an intermediate (bifunctional mechanism).

Electrocatalysts were also tested in a real cell fed with methanol and the results for Pt-Sn supported catalysts on VC and NT are shown in Figures 6a and 6b at two different temperatures and pressures in the cathode side and are compared with a commercial catalyst.

Polarization curves of Pt-Sn catalysts supported on VC and NT when tested at 70°C and atmospheric pressure (Figure 6a) are similar to that of the commercial catalyst, the open circuit potential being higher for both Pt-Sn catalysts than for the commercial one. The maximum power attained by both bimetallic catalysts is about 38 mW/cm^2. Such maximum for Pt-Sn/VC catalyst is placed at 0.25 A/cm^2 whereas for the Pt-Sn/NT catalyst, it is placed at 0.18 A/cm^2. For the commercial catalyst the maximum power (32 mW/cm^2) is at the same current density than for Pt-Sn/VC catalyst. On the other hand, Figure 6b shows the behavior at 90°C and 2 atm oxygen pressure in the cathode, and it can be seen that the performance of the electrocatalysts under these operating conditions is better than the one at 70°C and atmospheric pressure in the cathode. This fact is due to that the higher the pressure on the cathodic side, the higher the power developed because the methanol crossover through the membrane decreases. In this case, the power given by bimetallic catalysts clearly increases up to about 70 mW/cm^2 with the maximum between 0.3-0.35 A/cm^2, whereas the commercial catalyst only reaches a maximum of 60 mW/cm^2 at 0.4 A/cm^2. As it can be observed in Figure 6b, at low current density the performance of the DMFC with Pt-Sn/VC and Pt-Sn/NT catalysts is better than with the commercial one. At low current density zones where methanol oxidation is not so fast and its chemical adsorption is not the limiting reaction rate step, these bimetallic catalysts are more convenient for DMFC. However, they do not show a good behavior at high current densities.

These results of Pt-Sn catalysts supported on VC and NT agree with the ones reported by Colmatti et al.[25] finding that there could be obtained better results in DMFC with Pt-Sn catalysts than pure Pt ones under two conditions: i) moderate alloy formation and ii) operating the cells at low current densities. According to these authors, there would exist a poor methanol adsorption/dehydrogenation due to the presence of a fraction of Sn alloyed with Pt. As a consequence, at low current density, little amounts of methanol are necessary to operate the cell and in these conditions the methanol adsorption/dehydrogenation can take place more easily, the adsorbed CO oxidation being the limiting step of the methanol oxidation reaction (MOR). In increasing the methanol consumption at high current densities, methanol adsorption/dehydrogenation is turned to be the MOR limiting step and the power density falls quickly.

It could be suggested that the bimetallic Pt-Sn catalyst supported on mesoporous carbon and prepared by this technique of deposition-reduction in liquid phase with sodium borohydride shows a metallic phase with an important Pt blocking by Sn, this reducing the hydrogen chemisorption capacity and hindering the CO adsorption during cyclic voltammetric tests.

Moreover the metallic phase of Pt-Sn catalysts supported on Vulcan carbon and carbon nanotubes and similarly prepared give rise to a metallic phase where there would exist both geometric effects such as dilution and electronic ones, especially for those catalysts supported on Vulcan carbon. These surface modifications would give the active metal an important promoting effect that makes the CO electrochemical oxidation to take place more easily at lower potentials. The performance of the DMFC with both electrocatalysts (Pt-Sn/VC and Pt-Sn/NT) was better than with a commercial one in low current density working zones where methanol electro-oxidation is not so fast and its chemical adsorption is not the limiting reaction rate step.

Conclusions

The liquid phase deposition-reduction method with sodium borohydride (RB) to prepare bimetallic Pt-Sn catalysts gives a good Pt reducibility, and shows the presence of oxidized Sn species. A small fraction of the second metal (10–15%) stays in zerovalent state probably forming alloys.

For Vulcan carbon and carbon nanotubes as supports, it was found a low Pt-second metal electronic interaction but an important geometric effect that causes the promoting effect of Sn over Pt.

By using this preparation method, Pt-Sn catalysts supported on mesoporous carbon did not show an adequate electrochemical behavior because of strong blocking effects of the active metal by the second one.

As Sn is found in the vicinity of small Pt particles, it is produced an important promoting effect that makes CO electrochemical oxidation easier since it shifts the onset potential to lower values.

When tested in a DMFC, these Pt-Sn catalysts supported on VC and NT gave a better power density than a commercial one only at low current densities.

Acknowledgments

Authors thank Miguel A. Torres and Julieta Vilella for their assistance. Besides, this work was made with the financial support of Universidad Nacional del Litoral (Project CAI+D), CONICET (Project 970/09) and ANPCYT (Project PICT 2097, PAE 36985), and the Cooperation Project between Brazil and Argentina (Project Twinning).

References

1. Z. G. Shao, F. Zhu, W. F. Lin, P. A. Christensen, and H. Zhang, *Phys. Chem. Chem. Phys.*, **8**, 2720 (2006).
2. C. Lamy, A. Lima, V. LeRhun, F. Delime, C. Coutanceau, and J. M. Leger, *J. Power Sources*, **105**, 283 (2002).
3. R. Dillon, S. Srinivasan, A. S. Aricò, and V. Antonucci, *J. Power Sources*, **127**, 112 (2004).
4. D. H. Lim, W. D. Lee, and H. I. Lee, *Catal. Surv. Asia*, **12**, 310 (2008).
5. S. Song, W. Zhou, Z. Liang, R. Cai, G. Sun, Q. Xin, V. Stergiopoulos, and P. Tsiakaras, *Appl. Catal. B*, **55**, 65 (2005).
6. H. A. Gasteiger, N. Markovic, P. N. Ross Jr, and E. J. Cairns, *J. Electrochem. Soc.*, **141**, 1795 (1994).
7. S. A. Lee, K. W. Park, J. H. Choi, B. K. Kwon, and Y. E. Sung, *J. Electrochem. Soc.*, **149**, A1299 (2002).
8. C. Kim, H. H. Kwon, I. K. Song, Y. E. Sung, W. S. Chung, and H. I. Lee, *J. Power Sources*, **171**, 404 (2007).
9. M. Arenz, V. Stamenkovic, B. B. Blizanac, K. J. Mayrhofer, N. M. Markovic, and P. N. Ross, *J. Catal.*, **232**, 402 (2005).
10. I. Honma and T. Toda, *J. Electrochem. Soc.*, **150**, A1689 (2003).
11. W. S. Cardoso, M. S. P. Francisco, A. M. S. Lucho, and Y. Gushikem, *Solid State Ionics*, **167**, 165 (2004).
12. F. Colmati, E. Antolini, and E. R. Gonzalez, *Appl. Catal. B*, **73**, 106 (2007).
13. E. Peled, T. Duvdevani, A. Aharon, and A. Melman, *Electrochem. Solid-State Lett.*, **4**, A38 (2001).
14. D. H. Lim, D. H. Choi, W. D. Lee, D. R. Park, and H. I. Lee, *Electrochem. Solid-State Lett.*, **10**, 87 (2007).
15. M. Götz and H. Wendt, *Electrochim. Acta*, **43**, 3637 (1998).
16. A. Oliveira Neto, M. J. Giz, J. Perez, E. A. Ticianelli, and E. R. Gonzalez, *J. Electrochem. Soc.*, **149**, A272 (2002).
17. J. S. Choi, W. S. Chung, H. Y. Ha, T. H. Lim, I. H. Oh, S. Hong, and H. Lee, *J. Power Sources*, **156**, 466 (2006).
18. Z. Liu, X. Y. Ling, X. Su, and J. Y. Lee, *J. Phys. Chem. B*, **108**, 8234 (2004).
19. T. C. Deivaraj, W. Chen, and J. Y. Lee, *J. Mater. Chem.*, **13**, 2555 (2003).
20. Z. Liu, B. Guo, L. Hong, and T. H. Lim, *Electrochem. Commun.*, **8**, 83 (2006).
21. J. Zeng and J. Yang Lee, *Int. J. Hydrogen Energy*, **32**, 4389 (2007).
22. S. Mukerjee and R. C. Urian, *Electrochim. Acta*, **47**, 3219 (2002).
23. N. M. Markovic, B. N. Grgur, C. A. Lucas, and P. N. Ross, *J. Phys. Chem. B*, **103**, 487 (1999).
24. M. Carmo, M. Brandalise, A. Oliveira Neto, E. V. Spinacé, A. D. Taylor, M. Linardi, and J. R. G. Poco, *Int. J. Hydrogen Energy*, **36**, 14659 (2011).
25. F. Colmati, E. Antolini, and E. R. Gonzalez, *Electrochim. Acta*, **50**, 5496 (2005).
26. J. H. Kim, S. M. Choi, S. H. Nam, M. H. Seo, S. H. Choi, and W. B. Kim, *Appl. Catal. B*, **82**, 89 (2008).
27. S. G. Ramos, A. Calafiore, A. R. Bonesi, W. E. Triaca, A. M. Castro Luna, M. S. Moreno, G. Zampieri, and S. Bengio, *Int. J. Hydrogen Energy*, **37**, 14849 (2012).
28. I. Borbáth, D. Gubán, Z. Pászti, I. E. Sajó, E. Drotár, J. L. Gómez de la Fuente, T. Herranz, S. Rojas, and A. Tompos, *Top. Catal.*, **56**, 1033 (2013).
29. M. J. Gonzalez, C. T. Hable, and M. S. Wrighton, *J. Phys. Chem. B*, **102**, 9881 (1998).
30. S. Beyhan, C. Coutanceau, J.-M. Léger, T. W. Napporn, and F. Kadırgan, *Int. J. Hydrogen Energy*, **38**, 6830 (2013).
31. H. Sun, L. Zhao, and F. Yu, *Int. J. Electrochem. Sci.*, **8**, 2768 (2013).
32. Z. L. Liu, B. Guo, L. Hong, and T. H. Lim, *Electrochem. Commun.*, **8**, 83 (2006).
33. A. L. Dicks, *J. Power Sources*, **156**, 128 (2006).
34. S. H. Joo, H. I. Lee, D. J. You, K. Kwon, J. H. Kim, and Y. S. Choi, *Carbon*, **46**, 2034 (2008).
35. Z. Lei, S. Bai, Y. Xiao, L. Dang, L. An, G. Zhang, and Q. Xu, *J. Phys. Chem. C*, **112**, 722 (2008).
36. S. H. Liu, W. Y. Yu, C. H. Chen, A. Y. Lo, B. J. Hwang, and S. H. Chien, *Chem. Mater.*, **20**, 1622 (2008).
37. J. H. Zhou, J. P. He, Y. J. Ji, W. J. Dang, X. L. Liu, G. W. Zhao, C. X. Zhang, J. S. Zhao, Q. B. Fu, and H. P. Hu, *Electrochim. Acta*, **52**, 4691 (2007).
38. E. P. Ambrosio, M. A. Dumitrescu, C. Francia, C. Gerbaldi, and P. Spinelli, *Fuel Cells*, **9**, 197 (2009).
39. M. M. Bruno, M. A. Petruccelli, F. A. Viva, and H. R. Corti, *Int. J. Hydrogen Energy*, **38**, 4116 (2013).
40. M. M. Bruno, N. G. Cotella, M. C. Miras, and C. Barbero, *Colloids Surf. A*, **362**, 28 (2010).
41. M. M. Bruno, H. R. Corti, J. Balach, G. N. Cotella, and C. A. Barbero, *Funct. Mater. Lett.*, **2**, 135 (2009).
42. J. Falconer and J. Schuwarz, *Catal. Rev-Sci. Eng.*, **25**, 141 (1983).
43. F. Maillard, M. Eikerling, O. V. Cherstiouk, S. Schreier, E. Savinova, and U. Stimming, *Faraday Discuss.*, **125**, 357 (2004).
44. N. Veizaga, J. Fernandez, M. Bruno, O. Scelza, and S. de Miguel, *Int. J. Hydrogen Energy*, **37**, 17910 (2012).
45. C. D. Wagner, W. M. Riggs, L. E. Davis, J. F. Moulder, and G. E. Muilenberg, *Handbook of X-ray Photoelectron Spectroscopy*, Perkin-Elmer Co., Physical Electronics (1979).
46. D. Poondi and M. A. Vannice, *J. Catal.*, **161**, 742 (1996).
47. G. Haller, *J. Catal.*, **216**, 12 (2003).
48. T. Vidakovic, M. Christov, and K. Sundamcher, *Electrochim. Acta*, **52**, 5606 (2007).
49. A. Oliveira Neto, R. R. Dias, M. M. Tusi, M. Linardi, and E. V. Spinacé, *J. Power Sources*, **166**, 87 (2007).